AAEC/E404

AAEC/E404

AUSTRALIAN ATOMIC ENERGY COMMISSION
RESEARCH ESTABLISHMENT
LUCAS HEIGHTS

CHARACTERISATION OF NEUTRON IRRADIATION DAMAGE IN ZIRCONIUM ALLOYS - A 'ROUND ROBIN' EXPERIMENT

by

P.M. KELLY
R.G. BLAKE
A. JOSTSONS

January 1977

ISBN 0 642 99765 9

AUSTRALIAN ATOMIC ENERGY COMMISSION
RESEARCH ESTABLISHMENT
LUCAS HEIGHTS

CHARACTERISATION OF NEUTRON IRRADIATION DAMAGE IN ZIRCONIUM ALLOYS - A 'ROUND ROBIN' EXPERIMENT

by

P.M. KELLY
R.G. BLAKE
A. JOSTSONS

ABSTRACT

The nature of the damage structure in the neutron-irradiated zirconium specimens supplied as part of an international 'Round Robin' experiment has been studied using transmission electron microscopy. The damage structure consists entirely of a/3 $<11\bar{2}0>$ dislocation loops and no evidence has been found for $\underline{c}$ component loops. Both vacancy and interstitial loops were found in specimens where inside/outside contrast analysis was possible. Quantitative measurements of loop size distributions and loop concentrations are reported. All specimens exhibited corduroy contrast to varying degrees.

National Library of Australia card number and ISBN 0 642 99765 9

The following descriptors have been selected from the INIS Thesaurus to describe the subject content of this report for information retrieval purposes. For further details please refer to IAEA-INIS-12 (INIS: Manual for Indexing) and IAEA-INIS-13 (INIS: Thesaurus) published in Vienna by the International Atomic Energy Agency.

BURGERS VECTOR; DISLOCATIONS; ELECTRON MICROSCOPY; INTERSTITIALS; MICROSTRUCTURE; NEUTRONS; PHYSICAL RADIATION EFFECTS; VACANCIES; ZIRCONIUM; ZIRCONIUM BASE ALLOYS

CONTENTS

CONTENTS(Continued)

1. INTRODUCTION

This report contains the results of the AAEC examination of irradiated zirconium specimens supplied to the participants in an international 'Round Robin' experiment. This experiment was suggested and organised by Dr. D.O. Northwood of Chalk River Nuclear Laboratories. The aim was for the participating laboratories to examine specimens taken from a set of irradiated samples. The specimens, in the form of discs suitable for electropolishing, were supplied from either crystal bar zirconium or Zircaloy-2 irradiated to a range of fast neutron fluences and temperatures. By eliminating specimen variation as a possible source of discrepancy between workers' results, it was hoped to settle some of the controversy still surrounding the nature of the defect clusters in irradiated zirconium alloys. In particular, the aim of this exercise was to settle the controversy regarding the presence of $\underline{c}$ component damage. Other parameters of the defect structure to be studied were: loop size, loop concentration and the nature of the loop population, *i.e.* vacancy or interstitial.

The following laboratories agreed to participate in the Round Robin.

i) Chalk River Nuclear Laboratories } Atomic Energy of Canada Ltd (AECL)
ii) Whiteshell } Atomic Energy of Canada Ltd (AECL)
iii) General Electric - Vallecitos - USA (G.E.)
iv) Berkeley Nuclear Laboratories - Central Electricity Generating Board, U.K. (CEGB)
v) Lucas Heights - Australian Atomic Energy Commission Research Establishment (AAECRE)

Specimens supplied by Chalk River and G.E. were sent to participating laboratories in September 1975. The irradiation history of the specimens is shown in Table 1.

2. EXPERIMENTAL DETAILS

The oxide film on the specimens was removed by polishing on 600 mesh SiC paper and thin foils for transmission electron microscopy were prepared by electropolishing. Two electropolishing techniques were employed. Most of the specimens were prepared by first dimpling the specimen on both sides with a jet of electrolyte at 203 K and 240 V. The electrolyte contained 6% perchloric acid in methanol. Final polishing was carried out in a glass beaker at 16 V with an electrolyte containing 2% perchloric acid, 5% butanol in methanol and maintained at 203 K. Specimens were also polished in a commercial automatic twin-jet unit manufactured by Struers in Denmark.

The electrolyte contained 6% perchloric acid, 32% butoxy ethanol in methanol. Polishing was carried out at 18 V with the electrolyte maintained at 223 K.

Thin foils were examined at 200 kV in a JSEM-200 fitted with a ± 45° double-tilt goniometer stage modified to give ± 50° tilt about one axis. In all cases, the specimen texture was such that the all important prism orientations and the critical (0002) reflection could be reached. Furthermore, the $\langle 11\bar{2}3\rangle$ orientation for loop characterisation was also attainable in all specimens.

All micrographs are printed with the emulsion side up and $+\ \underline{z}$ is antiparallel to the electron beam.

Foil thicknesses for quantitative determinations of loop concentrations were estimated from extinction contours or grain-boundary fringes. The relevant extinction thicknesses were calculated using a four-beam dynamical calculation and corrected for Debye temperature effects, using the atomic scattering factors given by Smith & Burge [1962]. The relevant extinction thicknesses are shown in Appendix A.

3. OBSERVATIONS

The results of this investigation will be described in three parts. First, we will deal with the Burgers vector analysis, then with the quantitative aspects and finally with general microstructural features of the damage structure.

3.1 Burgers Vector Identification

A complete account of the procedures necessary for the characterisation of dislocation loops in zirconium has been published elsewhere [Blake *et al.* 1976, Jostsons *et al.* 1976]. Here we are concerned mainly with establishing the presence or absence of loops with $\underline{c}$ component Burgers vectors. Obviously, this can be determined from the appearance of the micrographs taken with $\underline{g} = (0002)$. Loops with $\underline{c}$ component Burgers vectors will be in strong contrast, whereas loops with $\underline{b} = a/3\ \langle 11\bar{2}0\rangle$ will either be out of contrast or show residual contrast characteristic of $\underline{g}.\underline{b} = 0$ and $\underline{g}.\underline{b} \times \underline{u} \neq 0$. Unfortunately, in practice, the procedure is more complex because of the foil artefacts that may be responsible for some of the controversy which this Round Robin is attempting to resolve.

Our experience, and that of others [Bedford & Miller 1972, Northwood & Gilbert 1973, Carpenter & Northwood 1975], has shown that regardless of the foil preparation technique used, artefacts in the form of an oxide film and surface hydrides are always present. Optimisation of the foil preparation methods can minimise the extent of foil artefacts, but so far it has not been possible to eliminate them completely. The contrast from these artefacts can be confused with that expected from small defects or dislocation loops produced by fast neutron irradiation. Hence it is imperative that the nature of the artefacts and their contrast behaviour be understood.

The contrast from foil artefacts in zirconium has been discussed in the literature [Bedford & Miller 1972, Northwood & Gilbert 1973, Carpenter & Northwood 1975, Blake *et al.* 1976, Jostsons *et al.* 1976] but is not fully appreciated by all electron microscopists. Perhaps the most complete discussion of this contrast is given in our recent publications [Blake *et al.* 1976, Jostsons *et al.* 1976]. Here it is proposed to reiterate some of the arguments relating to artefact contrast and then to give simple rules which will aid in setting up diffraction conditions to minimise the interference from artefact contrast, without prejudicing the contrast from true radiation-induced defects.

The presence of an oxide film on zirconium foils can be demonstrated readily in dark field images of oxide reflections (Figure 1). The dark field image shows that the oxide consists of crystallites with diameters approximately 10 nm. In bright field images of the zirconium reflections, the oxide crystallites give rise to the mottled background structure which is characteristic of both irradiated and unirradiated zirconium imaged under conditions of small w. This mottled background structure with an apparent black dot size of 10 nm could be mistaken for contrast from small irradiation-induced defect clusters. It is normal practice to reduce the background mottle by increasing w until an appropriate compromise is reached between contrast from dislocations and loops and that from the background. Our experience is that suitable images with $\underline{g} = (11\bar{2}0)$ are obtained for $w \approx 1.5$. The exact value varies from foil to foil and depends on the specimen thinning technique. As stated elsewhere [Blake *et al.* 1976, Jostsons *et al.* 1976], the oxide contrast is believed to arise from strain fields associated with the lattice mismatch between the epitaxial oxide and the substrate foil.

Unfortunately, the required w values cannot be achieved for the critical reflection (0002). The maximum value of w is less than 0.8 for 200 kV electrons and about 0.9 for 100 kV electrons. To overcome this problem, we have resorted to using higher order reflections, such as (0004) and (0006), for which values of w equal to about 1.5 can be achieved. A similar approach could be taken with $\underline{g} = (10\bar{1}1)$ for which the maximum value of w is close to 1.0. This approach is open to the criticism that defects in the foil could be rendered invisible with higher values of w. Nevertheless, it is equally true that the use of (0002) reflections makes the identification of small defects equally suspect as the images could be readily confused with oxide contrast. Since it has not been possible to investigate the contrast behaviour of small dislocation loops in (0004) or (0006) reflections, we have argued that such defects would indeed be visible, because straight dislocations with c component Burgers vector are clearly observed and the residual contrast from b = a/3 $<11\bar{2}0>$ dislocations is visible [Jostsons *et al.* 1976]. In the present work, we have been able to locate a rare c component dislocation, presumably introduced by deformation prior to irradiation (Figure 2). On this basis, it is argued that the absence of dislocation loop contrast in (0004) or (0006) images with w less than 2.0 is sufficient proof that no c component dislocation loops are present.

Surface hydride precipitate is the other artefact on electropolished foils of zirconium. Our experience is that the amount of precipitate present is slightly higher in irradiated than unirradiated specimens, and that hydride formation is far more serious on Zircaloy-2 foils than in pure zirconium. Many of the features of surface hydrides are illustrated in Figure 3. The hydride precipitation is purely a surface phenomenon as can be deduced from the lack of dependence of precipitate density on foil thickness. In fact, the hydride density is often highest in the very thin parts of the foil. Since the hydride precipitate is located near the foil surfaces, the strain field images will be anomalous and their behaviour with reversal of g will differ from that expected from dislocation loops which show 'inside-outside' double arc images. This feature is discussed in greater detail elsewhere [Blake *et al.* 1976, Jostsons *et al.* 1976].

It must be acknowledged that there may be situations where it will be difficult to distinguish hydride images from those of dislocation loops. A particularly difficult case is one in which the damage defects are of a size where the contrast can be described as 'black-dot'. The black-dot defects will show anomalous black-white behaviour near foil surfaces but it would be most unlikely that all such defects would be located near foil surfaces in foils prepared from neutron-irradiated material. Thus, situations where all defects behave as if they are near foil surfaces would lead to suspicion of hydride formation. Variation of defect density with foil thickness will also aid in the detection of hydride precipitate.

Finally, since the oxide and hydride reflections may frequently lie very close to zirconium reflections in reciprocal space, complex moiré patterns may be observed. Figure 4 shows moiré fringes associated with surface hydride precipitates. Such images could lead the unwary to suspect and hypothesise the presence of faulted loops. Closer examination, however, permits a distinction to be made between these two effects. The spacing of fault fringes depends on the effective extinction distance, *i.e.* the reflection used and the value of w. The spacing of moiré fringes is not sensitive to w and is predominantly affected by the lattice mismatch of the hydride and zirconium matrix.

Having discussed contrast from foil artefacts let us return to the main theme of dislocation loop Burgers vectors. Figure 5 contains representative micrographs from all samples in the Round Robin imaged in a $[1\bar{1}00]$ orientation with $\underline{g} = (11\bar{2}0)$ and (0006). Loops aligned in rows parallel to the (0001) trace are visible in $(11\bar{2}0)$ images whereas the (0006) images show contrast from hydride precipitates only. From a number of similar micrographs of each specimen, it is concluded that *no* $\underline{c}$ component dislocation loops exist in these specimens. From our other work [Blake *et al.* 1976, Jostsons *et al.* 1976] it is clear that the damage consists solely of $a/3 \langle 11\bar{2}0 \rangle$ loops.

3.2 Quantitative Results

This section presents the results of loop size spectrum measurements and loop characterisation into vacancy and interstitial components. The loop nature can be established from the determination of 'inside/outside' contrast behaviour with reversal of the sign of $\underline{g}$, keeping w positive. A number of variants of the technique are available, but all rely heavily on a knowledge of the loop Burgers vector $\underline{b}$ and the position of the loop normal $\underline{n}$. The determination of both $\underline{b}$ and $\underline{n}$ requires the use of a series of tilting experiments during which the behaviour of a particular loop is investigated. In practice, owing to high loop concentrations and small loop sizes, it is often impossible to follow the behaviour of a given loop during a tilting sequence and hence many loops cannot be characterised. Consequently, we used the Kelly & Blake [1973] variant of the safe orientation method which, together with the known spread of loop habit planes [Blake *et al.* 1976, Jostsons *et al.* 1976], is the most attractive and practical approach. That is, the vacancy or interstitial nature of the loop is derived from the analysis of image shifts with $\underline{g} = \pm\,(\bar{1}\bar{1}22)$ in two-beam micrographs taken with $\underline{z}$ near a $\langle 11\bar{2}3\rangle$ orientation. Interstitial loops are in outside contrast when $\underline{g}$ (w positive) points towards [0001] on the Kikuchi map. A more detailed discussion of the procedure is given elsewhere [Blake *et al*. 1976].

A complete characterisation of the loops was possible only in sample B. Figure 6 shows the relevant $\pm\,\underline{g} = (1\bar{1}22)$ micrographs. In sample C, small loop sizes and a high loop concentration gave rise to excessive image overlap. Nevertheless, by using weak beam ($\underline{g}/2\underline{g}$ or $\underline{g}/3\underline{g}$) dark field imaging with $\pm\,\underline{g} = (11\bar{2}2)$, near $\underline{z} = \langle 11\bar{2}3\rangle$, a considerable number of loops could be identified (Figure 7). The loop size spectra of characterised loops in specimens B & C are shown in Figure 8. The vacancy or interstitial nature of loops could not be determined in samples A and G (Figure 9) because the loops were too small and too numerous for the inside/outside contrast analysis. The loops were sized, however, and the histograms of size distribution are shown in Figure 10.

The above size distributions refer to measurements on $\langle 11\bar{2}3\rangle$ foils. The loop diameter is thus intermediate between the 2a and 2b axes of elliptical loops [Blake *et al*. 1976, Jostsons *et al*. 1976]. In the case of sample B, the loop population is completely specified because *all* loops in a given field were measured. This was not the case for sample C where the results are a selective collection of those loops for which an unambiguous image shift was obtained. Most of the loops in a given foil could not be characterised. Since loops in zirconium, particularly vacancy loops in excess of 40 nm, are elliptical, we also present histograms of size measurements carried out at a prism orientation for specimens B and C where the loop size is now characterised by 2a (Figure 11).

For purposes of intercomparison, the raw data are also presented in tabular form in Appendix B and a summary of the loop parameters is given in Table 2.

3.3 Corduroy and Loop Alignment

The contrast effect termed 'corduroy', was found in all samples, (Figure 12). The contrast behaved in the manner described in detail elsewhere [Kelly *et al*. 1976], where it was demonstrated that corduroy is a thin foil artefact caused by foil relaxation due to long range stress fields of $a/3\ \langle 11\bar{2}0\rangle$ dislocation loops aligned in bands parallel to (0001) plane. There is no need to invoke a peculiar $\underline{c}$ component damage to explain the electron microscope contrast behaviour of corduroy, particularly as no evidence can be found for the existence of $\underline{c}$ component loops in specimens exhibiting corduroy.

The loop alignment necessary for the corduroy model [Kelly *et al.* 1976] was found in all samples. This alignment is obvious in prism-oriented foils imaged in $(11\bar{2}0)$ and $(20\bar{2}0)$. Since the loop alignment is not perfect, and there is a spectrum of loop sizes in a given specimen, the alignment is best revealed in the thinner regions of a foil. In samples A and G where the loops are very small and numerous, weak beam dark field microscopy may be used to render the alignment more obvious (Figure 13).

Finally, the corduroy spacing is obviously a function of loop size and foil orientation.

3.4 Loop Ellipticity

Elsewhere [Blake *et al.* 1976], we have shown that dislocation loops in zirconium are elliptical with the major axis approximately parallel to [0001], whereas the minor axis lies within the basal plane. It is important to realise that the loops are not circular - otherwise false conclusions can be reached regarding the loop normal and because of this, erroneous loop characterisation could result. An appreciation of loop ellipticity is also important if valid comparisons of loop size determinations are desired.

We have measured the loop ellipticities on some loops as a check on our results reported for zone-refined zirconium irradiated at similar temperatures but to a lower fast neutron fluence. These measurements could be made only on specimens from sample B and the results are shown in Figure 14. The overall trend in the behaviour of loop ellipticity, b/a, with loop size and character is consistent with our recent work [Blake *et al.* 1976, Jostsons *et al.* 1976]. Nevertheless, the scatter may be greater, particularly as more vacancy loops are observed with $b/a > 1$ and some of the interstitial loops show greater ellipticity than is expected from the earlier results. This behaviour is most likely due to increased loop interaction in specimen B which has a higher loop concentration than present in specimens examined previously. Obviously, the coalescence of two neighbouring loops within the band will lead to a high b/a value whereas the coalescence of two loops in neighbouring bands of aligned loops will give a small b/a ratio.

Owing to the foil texture, the loops could not be examined at both basal and prism orientations for a direct determination of loop ellipticity. Here we have used the method described by Kelly & Blake [1974] whereby the loops are examined at $\langle 11\bar{2}0\rangle$ and $\langle 10\bar{1}0\rangle$ orientations to deduce the true loop widths from which the b/a ratio can be derived since the foil tilts are carried out about the major axis of the loops.

3.5 Loop Habit Plane

Previous work [Blake *et al.* 1976, Jostsons *et al.* 1976] has shown that dislocation loops in zirconium are non-edge in character with the loop normal being tilted by up to 30° from the edge orientation towards one of the neighbouring $<10\bar{1}0>$ directions with an additional tilt towards [0001]. The results of some determinations on specimens from sample B are shown in Figure 15. This behaviour is consistent with our previous work on zone-refined zirconium and validates our use of the 'safe/unsafe' orientation variant for deriving loop character.

4. DISCUSSION AND CONCLUSIONS

The results of the examination of the Round Robin zirconium specimens have shown that:

1. *No* evidence for $\underline{c}$ component dislocation loops was found. Thus, under the conditions of temperature, fluence and specimen purity employed, only $a/3 <11\bar{2}0>$ loops were encountered.
2. In the two specimens (B and C) where the loops were sufficiently large for characterisation by the inside/outside contrast analysis, both vacancy and interstitial loops were present.
3. All specimens exhibited corduroy contrast to varying degrees.
4. Alignment of the $a/3 <11\bar{2}0>$ loops in bands parallel to the (0001) plane was observed in all specimens.
5. Quantitative data on loop size spectra, and loop concentration were obtained for all specimens. In the case of specimen B, the loops were characterised completely whereas in specimen C only a partial characterisation could be made.

These results are similar to those reported by us previously on zone-refined zirconium irradiated over a range of temperature and fluence. In particular, no evidence of $\underline{c}$ component dislocation loops was found. We have examined [Jostsons *et al.* 1976] previous claims in the literature [Lee & Koch 1974, Adamson *et al.* 1974, Gelles & Harbottle 1974, Riley & Grundy 1972] for the existence of $\underline{c}$ component loops and will not repeat the detailed arguments here. In all cases, the analysis of the electron microscope image contrast lacks sufficient rigour. Frequently, the supposed $\underline{c}$ component loop identification resulted from artefact contrast being confused with loop images. Finally, Bell [1975] has argued that corduroy is evidence for $\underline{c}$ component damage. However, we have demonstrated clearly

[Kelly *et al.* 1976] that corduroy is present in specimens where all the loops have a/3 $\langle 11\bar{2}0\rangle$ Burgers vectors and have proposed a model which explains all features of corduroy contrast, without invoking $\underline{c}$ component damage. In terms of this model of corduroy contrast, corduroy is a thin foil artefact associated with local relaxation of the thin foil in areas where there is pronounced alignment of a/3 $\langle 11\bar{2}0\rangle$ loops. This alignment of a/3 $\langle 11\bar{2}0\rangle$ loops in bands parallel to (0001) appears to be a fairly general feature of the damage structure in irradiated zirconium and hence corduroy is equally common.

5. REFERENCES

Adamson, R.B., Bell, W.L. & Lee, D. [1974] - Zirconium in Nuclear Applications. ASTM-STP 551, p.215.

Bedford, A.J. & Miller, D.R. [1972] - *J. Aust. Inst. Met.*, 17:120.

Bell, W.L. [1975] - *J. Nucl. Mater.*, 55:14.

Blake, R.G., Jostsons, A. & Kelly, P.M. [1976] - AAEC/E374.

Carpenter, G.J.C. & Northwood, D.O. [1975] - to be published in Proc. Intern. Conf. on Fundamental Aspects of Radiation Damage in Metals, Gatlinburg, Tenn. U.S.A., Oct. 5-10.

Gelles, D.S. & Harbottle, J.E. [1974] - CEGB RD/B/N2973.

Jostsons, A., Kelly, P.M. & Blake, R.G. [1976] - submitted to *J. Nucl. Mater.*

Kelly, P.M. & Blake, R.G. [1973] - *Philos. Mag.*, 28:415.

Kelly, P.M. & Blake, R.G. [1974] - *Phys. Status Solidi*, A25:599.

Kelly, P.M., Blake, R.G. & Jostsons, A. [1976] - *J. Nucl. Mater.*, 59:307.

Lee, D. & Koch, E.F. [1974] - *J. Nucl. Mater.*, 50:162.

Northwood, D.O. & Gilbert, R.W. [1973] - *J. Aust. Inst. Met.*, 18:158.

Riley, A. & Grundy, P.J. [1972] - *Phys. Status Solidi.*, A14:239.

Smith, G.H. & Burge, R.E. [1962] - *Acta Cryst.*, 15:182.

TABLE 1

IDENTIFICATION OF MATERIALS FOR ROUND ROBIN

Capsule Identification	Alloy	Material Details		Fluence (n.m^{-2} (E > 1 MeV))
		Metallurgical Condition	Irrad. Temp. (°C)	
A	Zircaloy-2	Annealed (1 h/750°C)	$\simeq$ 250	3.1×10^{24}
B	Crystal Bar	Annealed (1 h/750°C)	$\simeq$ 400	1×10^{25}
C	Zircaloy-2	Annealed (1 h/800°C)	$\simeq$ 400	1×10^{25}
G	Zircaloy-2	Annealed (at 577°C)	$\simeq$ 342 *	1×10^{25} †

* Boiling Water Reactor (BWR) environment

† Flux 1×10^{18} n m^{-2} s^{-1}

TABLE 2

QUANTITATIVE RESULTS FOR ROUND ROBIN SPECIMENS

Parameter	Sample A	Sample B	Sample C	Sample G
Average Loop Density ($10^{22}m^{-3}$)	5.0	0.88	1.95	3.2
Range ($10^{22}m^{-3}$)	(4.5-5.5)	(0.71-1.04)	(1.7-2.2)	(3.1-3.2)
Loop size at prism orientation, *i.e.* 2a				
Mean diameter nm	-	54	23	-
Median diameter	-	50	21	-
Total loops measured	-	322	446	-
Loop size near <11$\bar{2}$3> foil				
Mean diameter nm	6.4	51	-	8.3
Median diameter	5.0	43	-	6.3
Total loops measured	529	455	-	374
Total loops identified near <11$\bar{2}$3> foil	-	435	150*	-
Mean diameter nm	-	52	32	-
Median diameter	-	44	28	-
Vacancy loops				
Mean diameter nm	-	50	30	-
Median diameter	-	42	27	-
% Vacancy loops	-	66	77	-
Total vacancy loops measured	-	287	115	-
Interstitial loops				
Mean diameter nm	-	57	38	-
Median diameter	-	47	35	-
% interstitial loops measured	-	34	23	-
Total interstitial loops measured	-	148	35	-

* Note that the identified loops represented a small fraction of the loops present in the field of view and hence the meaning of the results on loop character is not obvious.

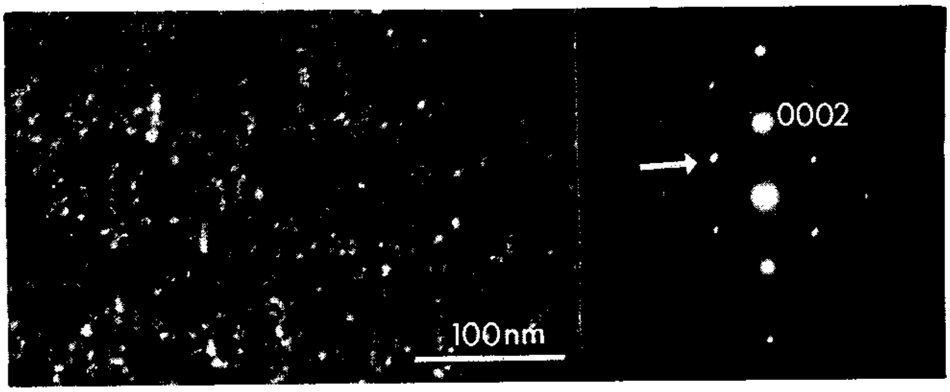

FIGURE 1 DARK FIELD IMAGE OF OXIDE REFLECTION (CIRCLED BY ARROWED APERTURE) SHOWING SURFACE OXIDE PARTICLES OF APPROXIMATELY 10 nm DIAMETER ($\underline{z} \approx [10\bar{1}0]$). SPECIMEN C.

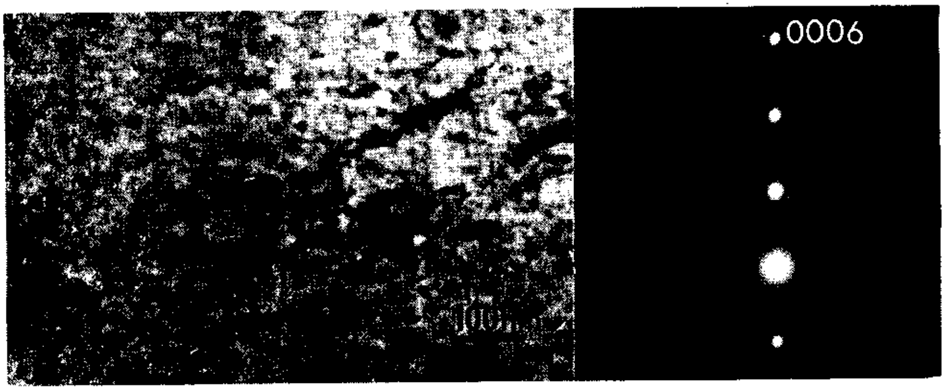

FIGURE 2 GROWN-IN $\underline{c}$ COMPONENT DISLOCATIONS IMAGED IN $\underline{g} = (0006)$.

Note the absence of contrast from irradiation-induced dislocation loops. (Specimen G, $\underline{z} \approx [10\bar{1}0]$).

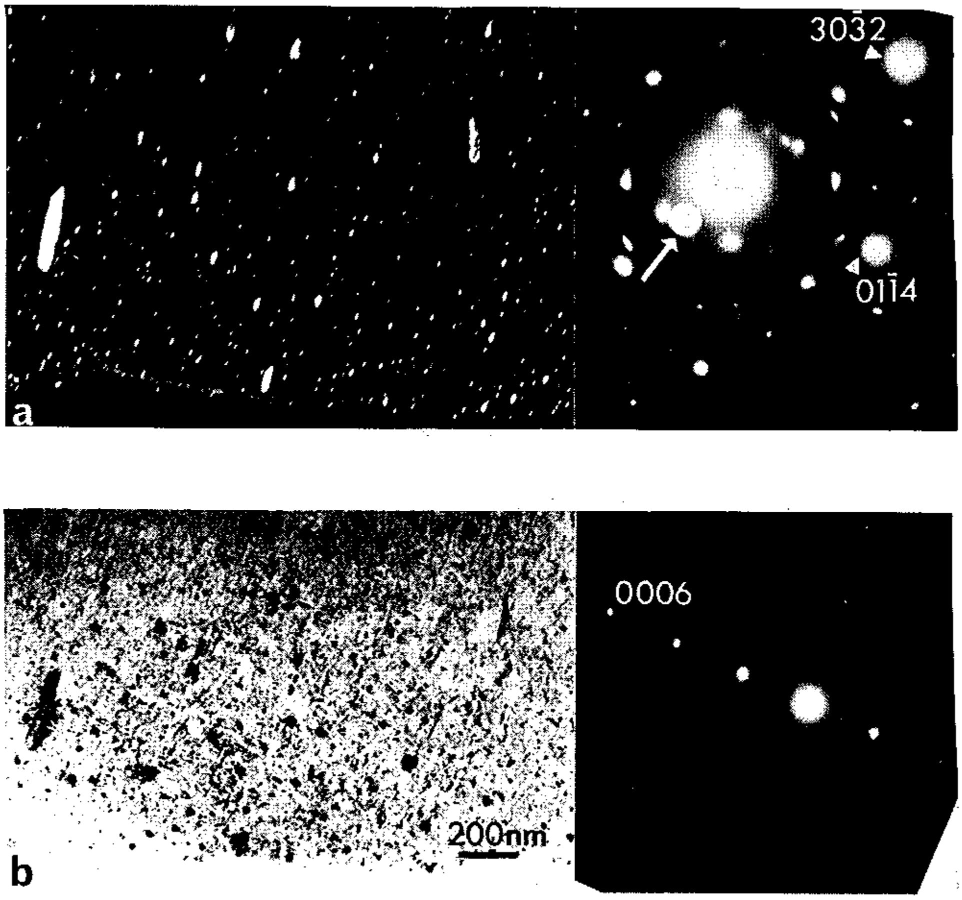

FIGURE 3 HYDRIDE PRECIPITATE PARTICLES IN ELECTROPOLISHED FOILS OF SPECIMEN C.

a) Dark field image of reflection circled by aperture, $\underline{z} \approx [1\bar{3}21]$.
b) Bright field image with $\underline{g} = (0006)$ at $\underline{z} \approx [10\bar{1}0]$.

Note that the hydride precipitate density is higher near the edge of the specimen than in the thicker parts of the foil. This behaviour shows clearly that the hydride precipitates are located at or near the foil surfaces and that hydride pickup during electropolishing is enhanced near specimen edges.

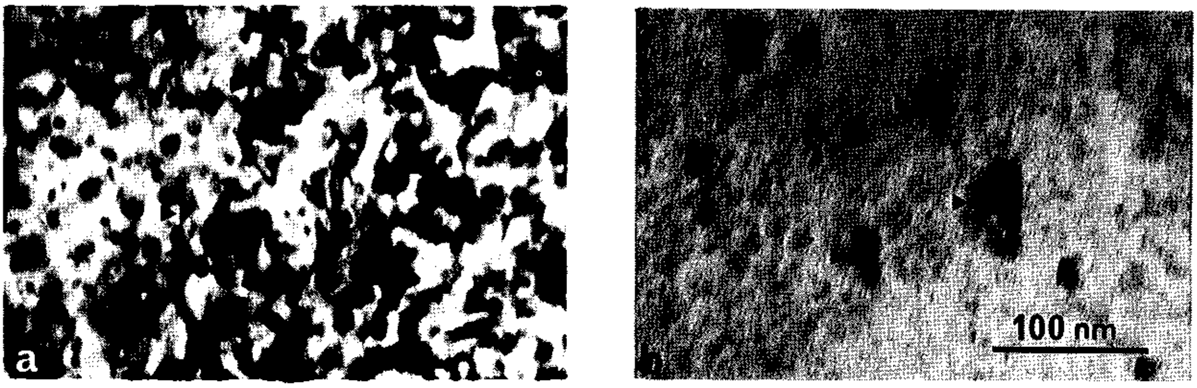

FIGURE 4 MOIRÉ FRINGES (ARROWED) FROM HYDRIDE PRECIPITATE AND NEUTRON INDUCED DISLOCATION LOOPS IN (a) IMAGED WITH $\underline{g} = (20\bar{2}2)$.

The hydride precipitate is revealed more clearly in (b) with $\underline{g} = (0006)$. ($\underline{z} \approx [1\bar{2}10]$, Specimen A).

FIGURE 5 THE MICROGRAPHS GIVE A COMPARISON OF THE SCALE OF THE DAMAGE STRUCTURE IN THE ROUND ROBIN SPECIMENS.

The lack of loop contrast in the (0006) images is proof of the absence of $\underline{c}$ component damage. All micrographs are at the same magnification and $z \approx [10\bar{1}0]$. (a) Specimen B, (b) Specimen C, (c) Specimen A and (d) Specimen G. Note that in the diffraction pattern of 5(c), the presence of the $(21\bar{3}\bar{5})$ reflection and others gives rise to the forbidden (0001) reflection by double diffraction. The additional reflections in 5(a) and (b) outside the (0001) row are due to the oxide.

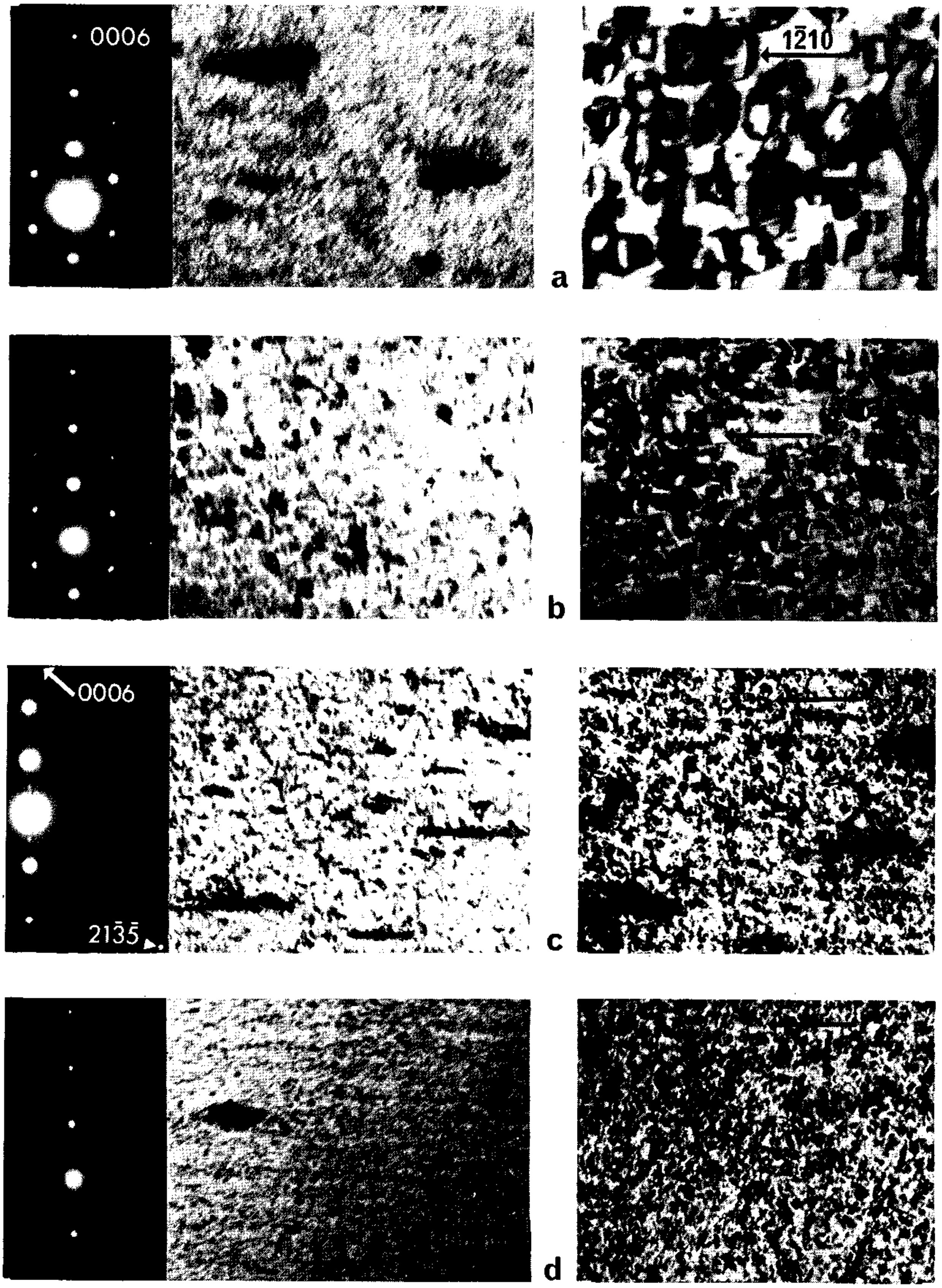

FIGURE 5 Caption

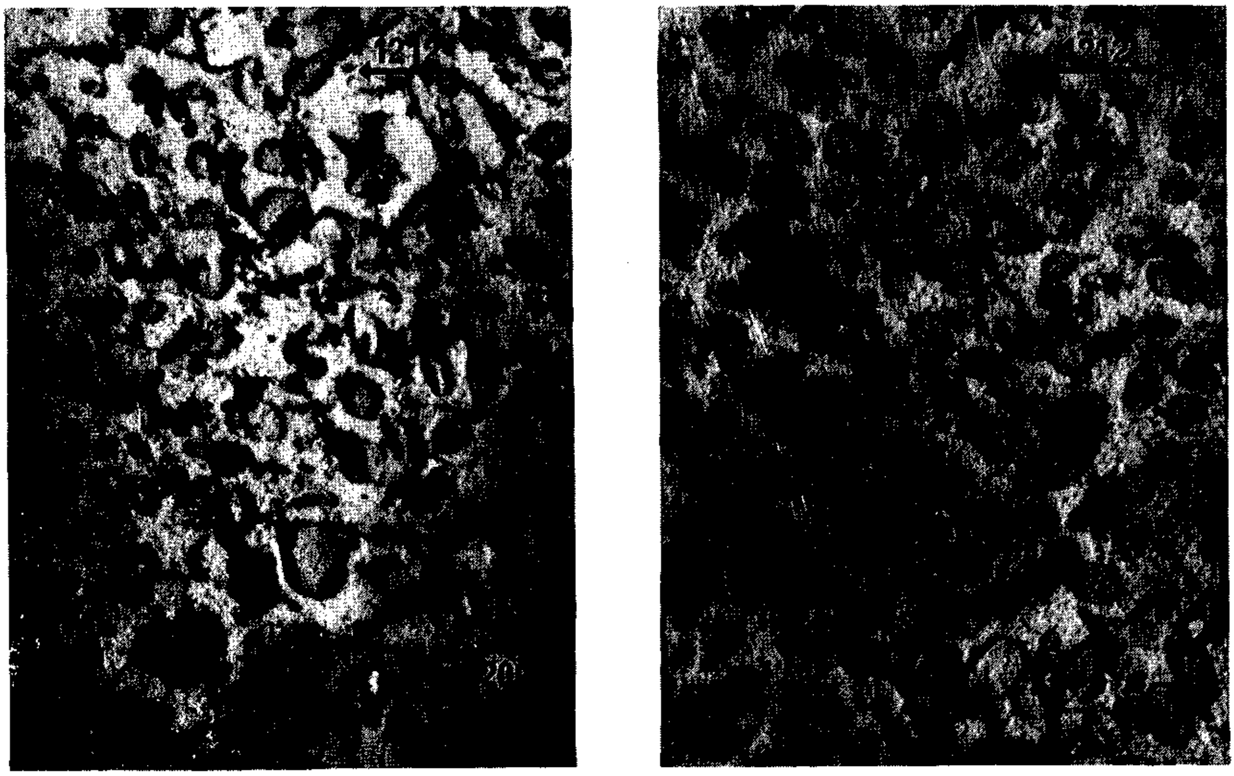

FIGURE 6 LOOPS IMAGED WITH ± g = $(1\bar{2}1\bar{2})$ at z ≈ $[1\bar{2}13]$.

Loops in outside contrast in (a) are interstitial. Specimen B.

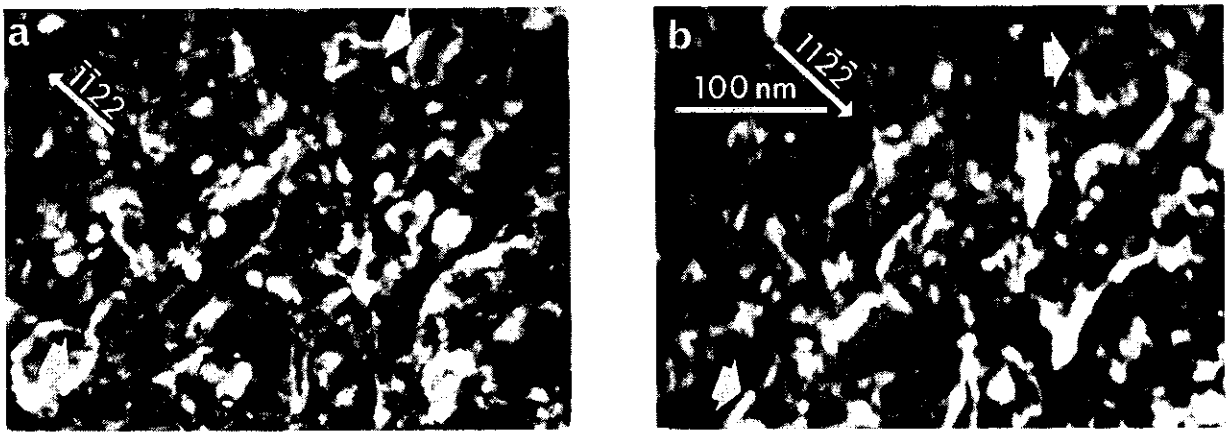

FIGURE 7 WEAK BEAM DARK FIELD g/2g, $\{11\bar{2}2\}$ IMAGES OF LOOPS IN SPECIMEN C AT z ≈ $<11\bar{2}3>$.

Loops in outside contrast in (a) are interstitial and those in outside contrast in (b) are vacancy. The loops arrowed are vacancy in character. As a result of the high loop density, image overlap renders the identification of individual loops difficult.

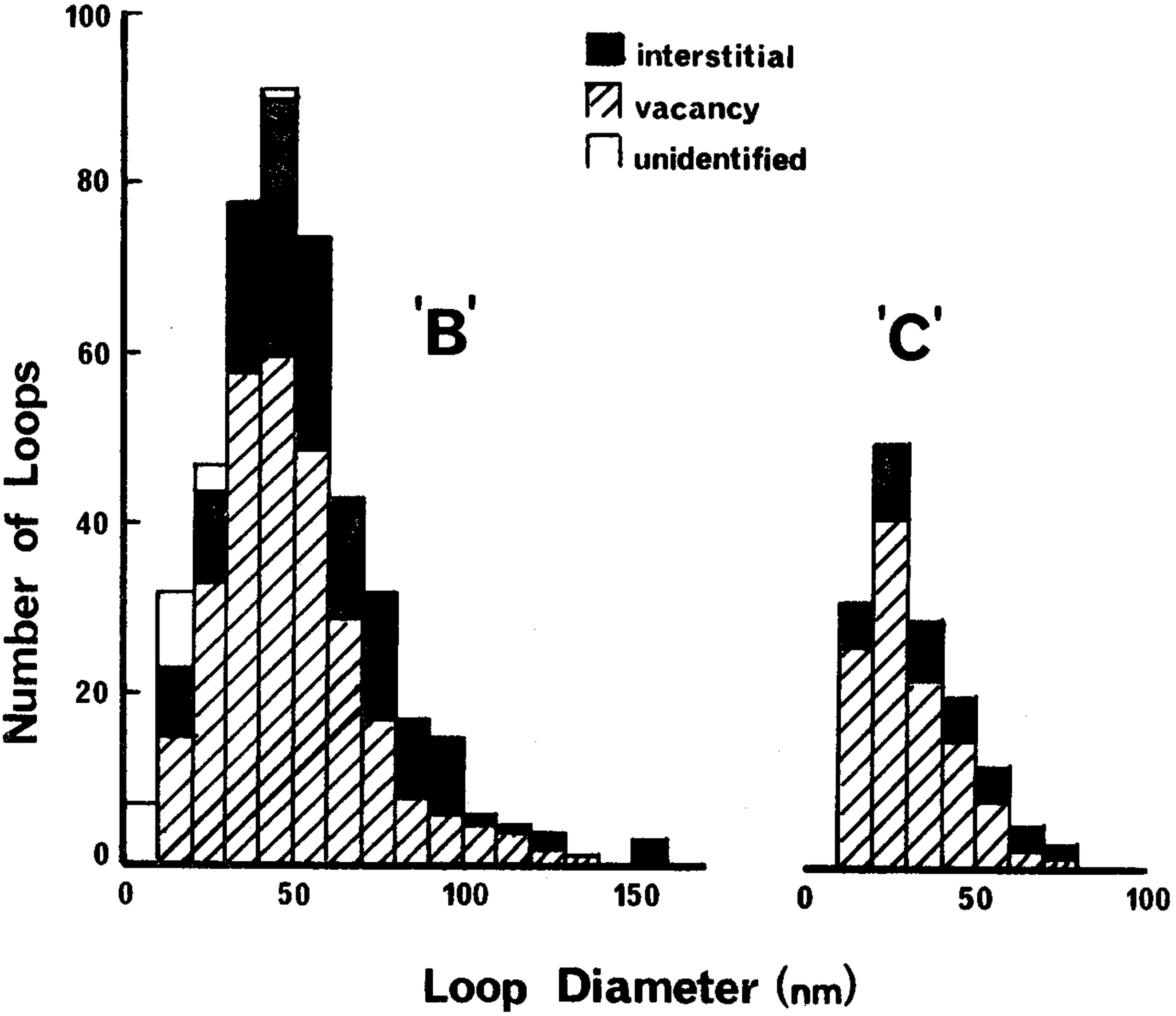

FIGURE 8 LOOP SIZE DISTRIBUTION PLOTS FOR SPECIMENS B AND C OBTAINED FROM $(11\bar{2}2)$ IMAGES AT $\underline{z} \approx \langle 11\bar{2}3 \rangle$.

The histogram for Specimen B is a true reflection of the size spectrum whereas that for Specimen C is a selective result obtained from a small fraction of loops present in a given region.

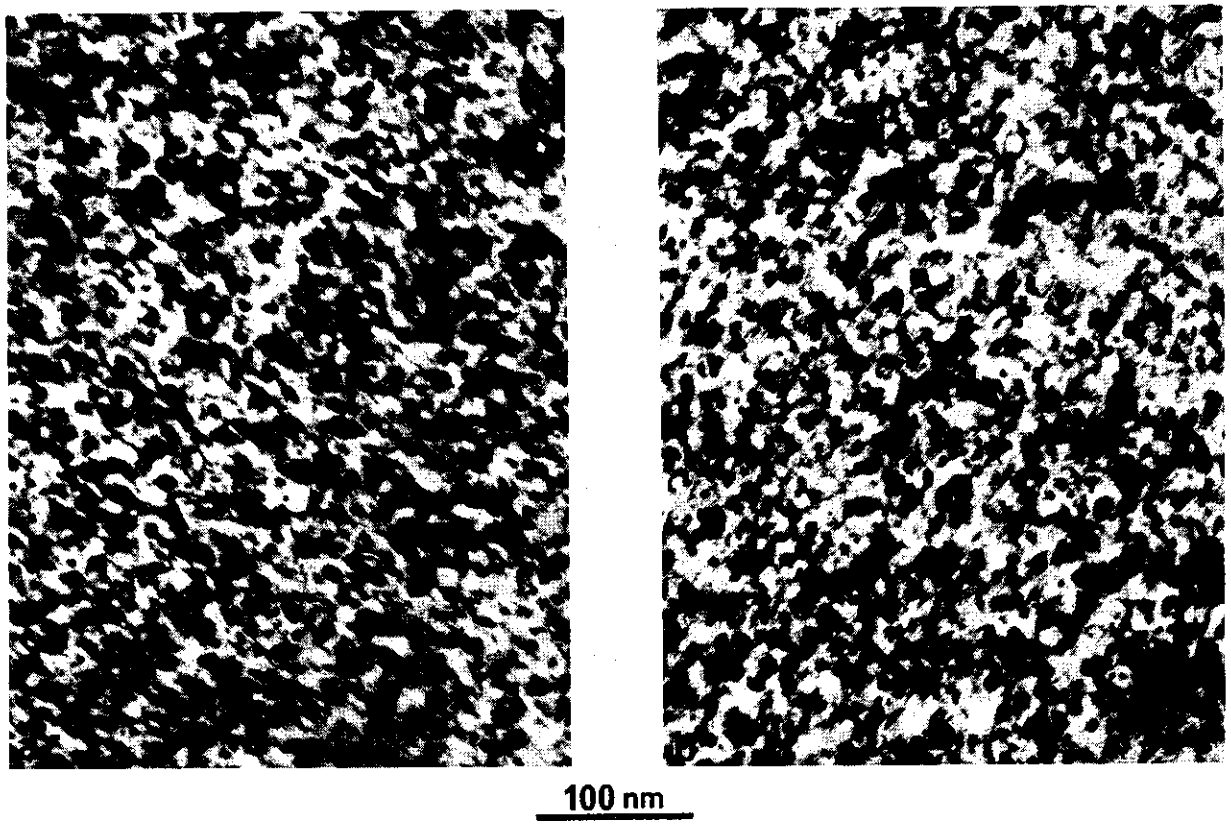

FIGURE 9 LOOP IMAGES OF SPECIMEN G (a) AND SPECIMEN A (b) NEAR $\underline{z} \approx \langle 11\bar{2}3\rangle$ AND $\underline{g} = (10\bar{1}1)$.

These loops are too small for identification using the conventional inside/outside image analysis.

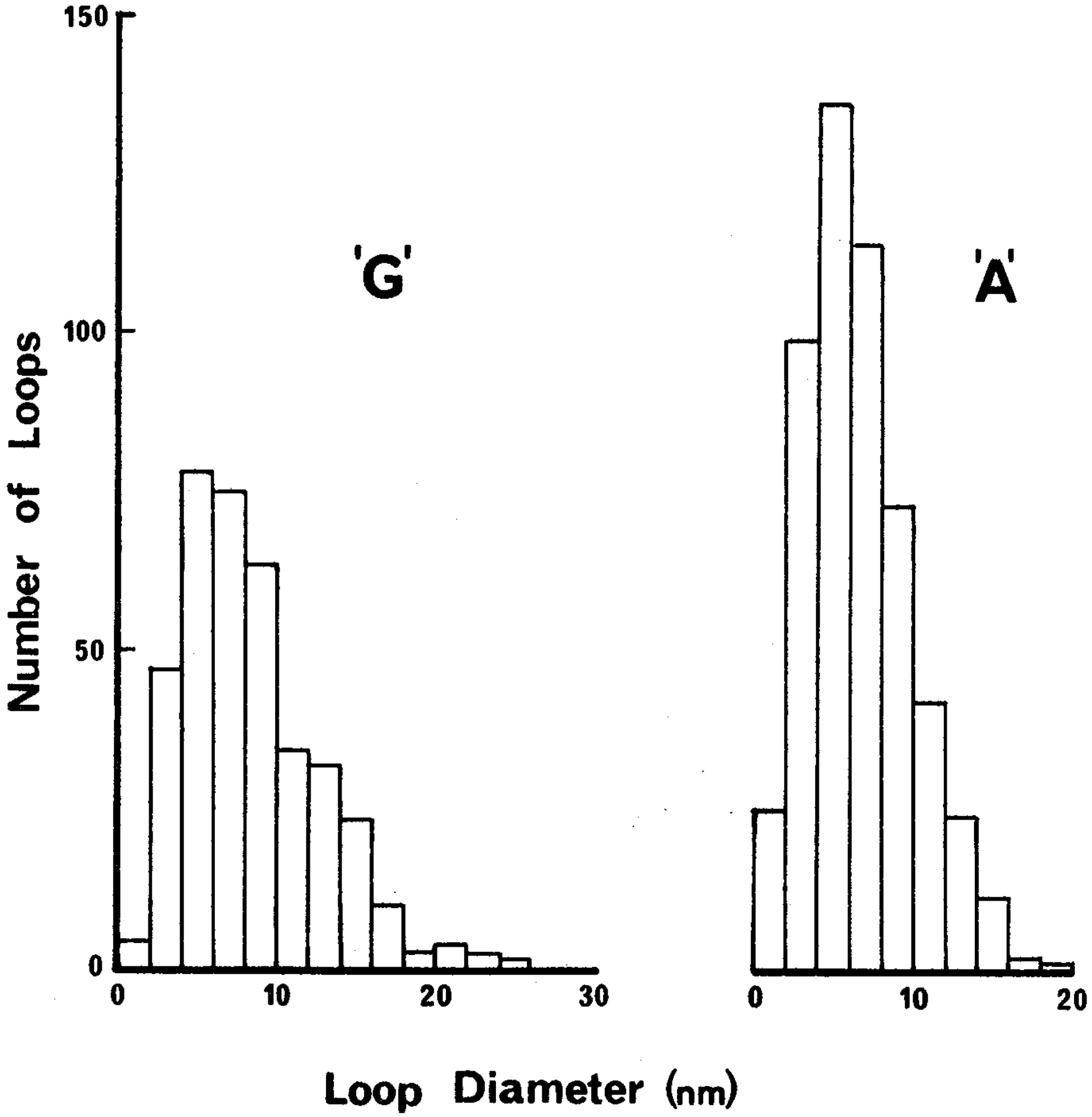

FIGURE 10 LOOP SIZE SPECTRA FOR SPECIMENS A AND G OBTAINED FROM $\underline{z} \approx <11\bar{2}3>$ FOILS.

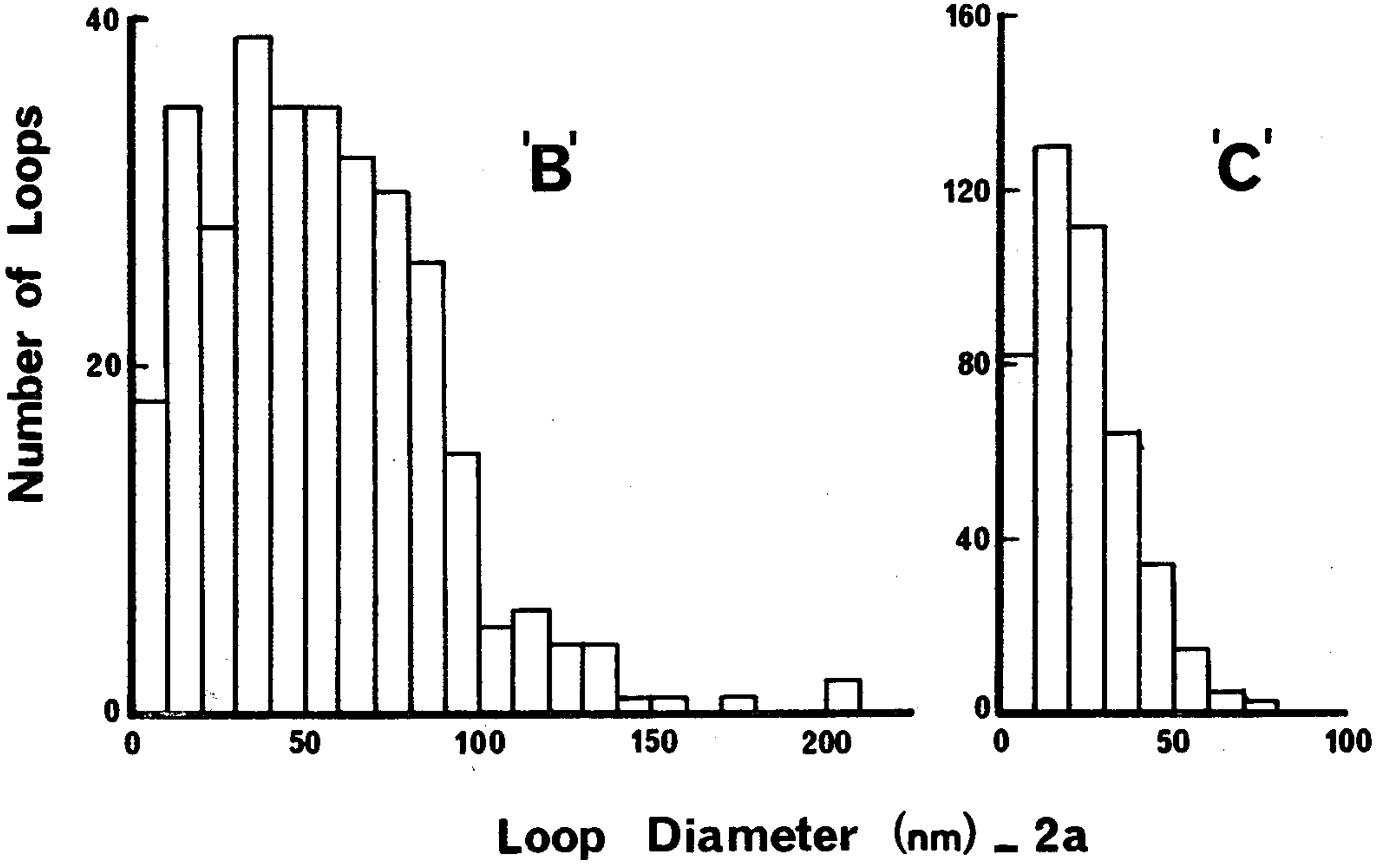

FIGURE 11 LOOP SIZE SPECTRA FOR SPECIMENS B AND C OBTAINED FROM $\underline{g} = (11\bar{2}0)$ IMAGES AT $\underline{z} \approx <10\bar{1}0>$.

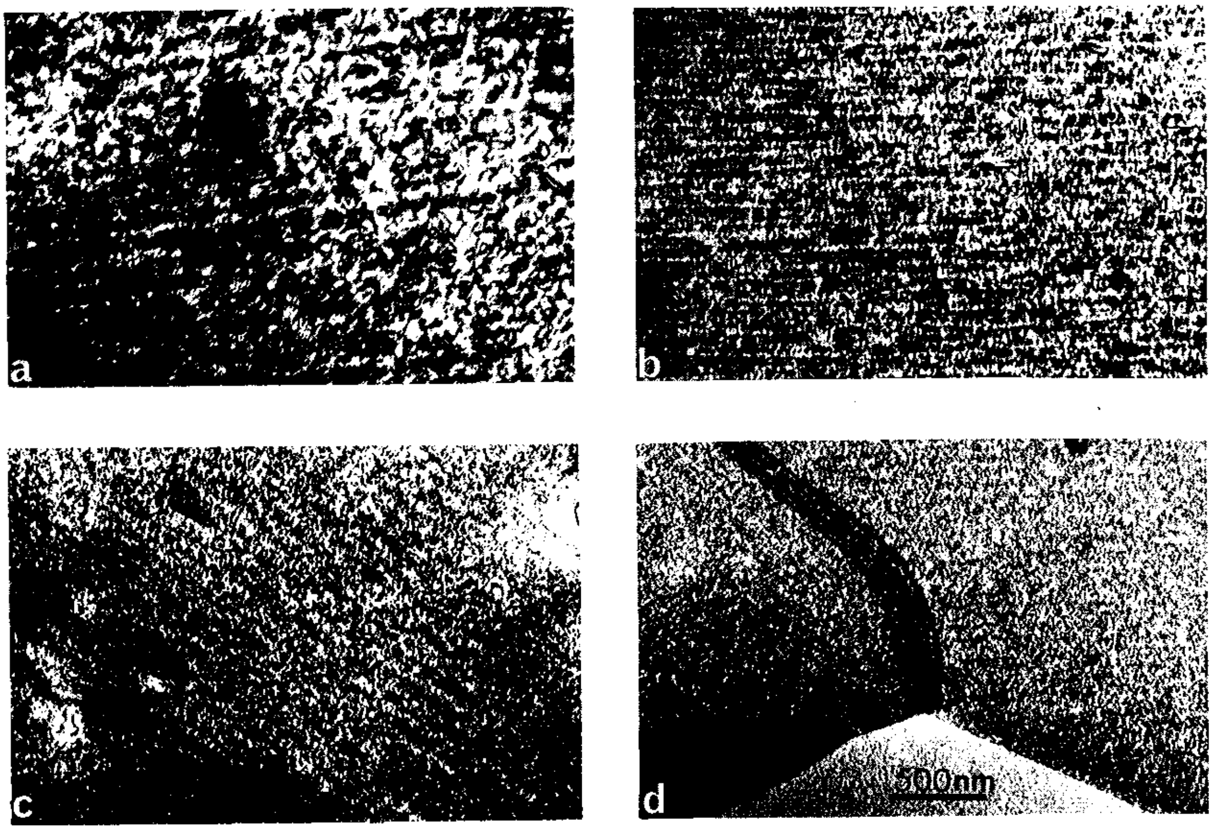

FIGURE 12 CORDUROY CONTRAST IN ROUND ROBIN SPECIMENS.

$\underline{z} \approx \langle 11\bar{2}3\rangle$ for a, c, and d, and $\underline{z} \approx \langle 10\bar{1}0\rangle$ for b. Specimens B (a), C (b), A (c) and G (d). All micrographs are at the same magnification.

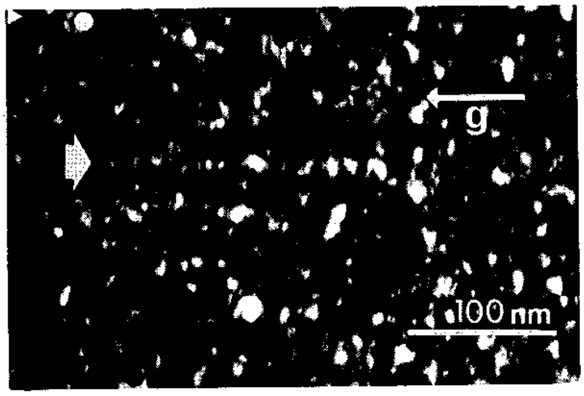

FIGURE 13 WEAK BEAM DARK FIELD $(11\bar{2}0)$ IMAGE OF LOOPS AT $\underline{z} \approx \langle 10\bar{1}0\rangle$ OF SPECIMEN A.

The alignment of loops in bands parallel to the (0001) trace is revealed more clearly (see row arrowed) than in the corresponding bright field image. (Figure 5(c)).

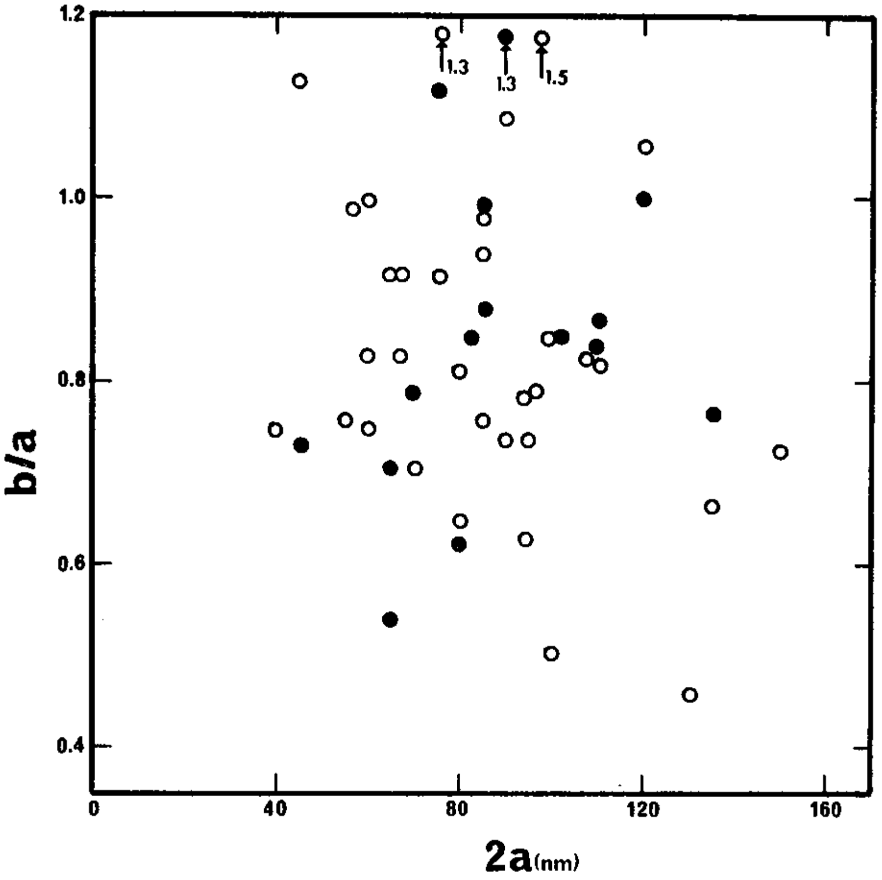

FIGURE 14 VARIATION OF LOOP ELLIPTICITY WITH LOOP SIZE AND CHARACTER IN SPECIMEN B.

Vacancy loops are represented by open circles and interstitial loops by full circles.

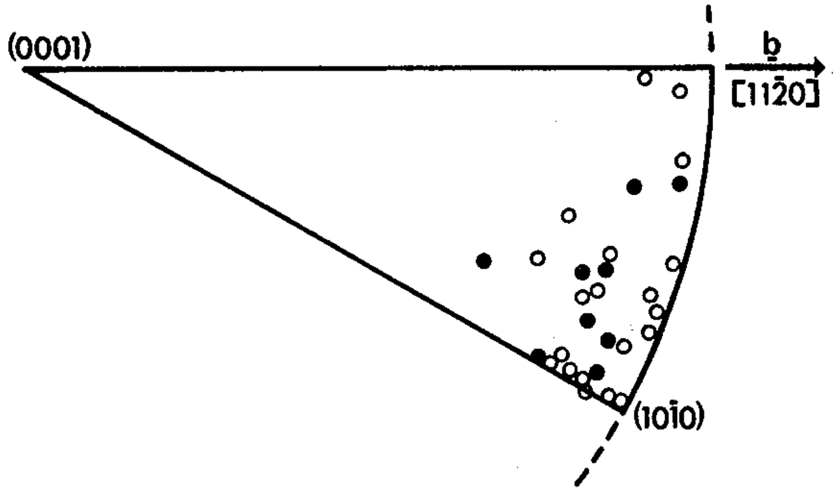

FIGURE 15 DISTRIBUTION OF LOOP PLANE NORMALS IN SPECIMEN B.

The loop Burgers vector has been taken to be a/3 [11$\bar{2}$0] and all results are plotted in a single triangle of the stereographic projection. Vacancy loops are represented by open circles and interstitial loops by full circles.

APPENDIX A*

EXTINCTION DISTANCES ξ_g (Å) IN α-ZIRCONIUM

FOUR-BEAM DYNAMICAL, DEBYE TEMPERATURE CORRECTED, AT 293 K

hkil	200 kV	100 kV
0002	345	272
$10\bar{1}0$	661	521
$10\bar{1}1$	463	365
$10\bar{1}2$	1051	829
$11\bar{2}0$	626	494
$11\bar{2}2$	779	614
$11\bar{2}4$	1211	955
$20\bar{2}1$	928	732
$21\bar{3}0$	2250	1774
$21\bar{3}1$	1342	1058

* These values were calculated by J.G. Napier according to the formulation given by A. Howie in 'Modern Diffraction and Imaging Techniques in Materials Science' (ed. S. Amelinckx, R. Gevers, G. Remaut & J. Van Landuyt) North-Holland Publishing Co., Amsterdam, 1970, p.308.
The Debye temperature correction was made using a value of $B = 0.45$ Å^2 obtained from 'International Tables for X-ray Crystallography', Vol. III, (ed. C.H. MacGillavry & G.D. Rieck) Kynoch Press, Birmingham, England, 1962, p.238.

APPENDIX B

LOOP SIZE DATA

B1 Specimen B

Size Interval (nm)	Number of Loops for $\underline{z} \approx \langle 10\bar{1}0\rangle$ (*i.e.* 2a)	Number of Loops for $\underline{z} = \langle 11\bar{2}3\rangle$		
		Vacancies	Interstitials	Unidentified
0-10	18	-	-	7
-20	35	15	8	9
-30	33	33	11	3
-40	39	58	20	-
-50	35	60	30	1
-60	35	49	25	-
-70	32	29	14	-
-80	30	17	15	-
-90	26	8	9	-
-100	15	6	9	-
-110	5	5	1	-
-120	6	4	1	-
-130	4	2	2	-
-140	4	1	-	-
-150	1	(> 150) -	3	-
-160	1			
-170	-			
-180	1			
-190	-			
-200	-			
> 200	2			
Total Number of Loops	322	287	148	20

B2 Specimen C

Size Interval (nm)	Number of Loops for $\underline{z}$ = <$10\bar{1}0$> (*i.e.* 2a)	Number of Loops for $\underline{z}$ = <$11\bar{2}3$>*	
		Vacancies	Interstitials
0-10	82	-	-
-20	130	26	5
-30	112	41	9
-40	65	22	7
-50	34	15	5
-60	15	8	1
-70	5	2	3
-80	3	1	2
Total	446	115	35

* The characterised loops are not representative of the full size spectrum as all loops within a region of the foil could not be sized. Consequently these data are highly selective.

B3 Specimens A and G

Size Interval (nm)	Number of Loops in Specimen A	Number of Loops in Specimen G
0-2	25	4
-4	99	47
-6	137	78
-8	114	75
-10	73	63
-12	42	34
-14	24	32
-16	12	23
-18	2	10
-20	1	2
-22		3
-24		2
-26		1
Total	529	334